Structure and photoluminescence properties of Er^{3+}-doped TiO_2–SiO_2 powders prepared by sol–gel method*

Zhao Jian-Guo(赵建果)[a)†], Zhang Wei-Ying(张伟英)[a)], Ma Zi-Wei(马紫微)[b)], Xie Er-Qing(谢二庆)[b)], Zhao A-Ke(赵阿可)[a)], and Liu Zhao-Jun(刘照军)[a)]

[a)] *College of Physics and Electronic Information, Luoyang Normal College, Luoyang* 471022, *China*
[b)] *School of Physical Science and Technology, Lanzhou University, Lanzhou* 730000, *China*

(Received 11 March 2011; revised manuscript received 19 April 2011)

Er^{3+}-doped TiO_2–SiO_2 powders are prepared by the sol–gel method, and they are characterized by high resolution transmission electron microscopy (HR-TEM), X-ray diffraction (XRD) spectra, and Raman spectra of the samples. It is shown that the TiO_2 nanocrystals are surrounded by an SiO_2 glass matrix. The photoluminescence (PL) spectra are recorded at room temperature. A strong green luminescence and less intense red emission are observed in the samples when they are excited at 325 nm. The intensity of the emission, which is related to the defect states, is strongest at the annealing temperature of 800 °C. The PL intensity of Er^{3+} ions increases with increasing Ti/Si ratio due to energy transfer between nano-TiO_2 particles and Er^{3+} ions.

Keywords: TiO_2–SiO_2, sol–gel, Raman, photoluminescence

PACS: 77.84.Lf, 78.55.Hx, 78.67.–n **DOI:** 10.1088/1674-1056/20/8/087701

1. Introduction

In recent years, there has been a renaissance in the study of rare-earth-doped materials for their possible applications in photoelectric devices, colour displays, and optical communication fields (i.e., flat panel displays, solid state lasers, high energy radiation detectors, optical data storage, etc.).[1−5] For these applications, inorganic oxide materials exhibit superior advantages in terms of their good chemical, thermal, and mechanical properties.[6−8] In this sense, glasses have proved to be useful as host materials for rare-earth elements because of their high transparency, compositional variety, and easy mass production. Nanoparticles embedded in glassy matrixes show promising applications in optical devices.[9]

Rare-earth erbium (Er) ions have been used widely because of their unique spectral properties, which include multiple emissions in the visible and infrared regions. When embedded in a solid matrix, erbium is generally assumed to be in the trivalent Er^{3+} state, which has an electronic configuration $[Xe]4f^N$. Spin–spin and spin–orbit couplings in the incompletely filled 4f shell give rise to a number of energy levels. Each degenerate level is Stark-split into a manifold of levels, due to an interaction between the ions and the host material.[10]

Titanium oxide (TiO_2) is an important oxide semiconductor that can be applied in the fields of photocatalytics, solar energy cells, self-cleaning, etc.[11−14] TiO_2 possesses a high refractive index, and physical and chemical stability. Therefore it is a good candidate to be used as a host material for other oxides. The interest in the sol–gel technique is due to several advantages, i.e., good homogeneity, control in sample composition, low processing temperature, and low equipment costs. The sol–gel method is believed to be a very effective and controllable route to future nanoparticle preparation. Binary mixed oxides TiO_2–SiO_2 have been synthesized through the sol–gel technique and investigated for various optical applications, such as anti-reflective coatings, planar optical waveguides, optical filters, and optical sensors.[15−18] However, rare-earth ion doped mixed oxide TiO_2–SiO_2 has rarely been reported. It is thus of significance to study the optical properties and local structures of the Er^{3+}

*Project supported by the Key Science and Technology Program of Henan Province of China (Grant Nos. 102102210448 and 102102210452) and the Scientific Research Fundation of the Education Department of Henan Province, China (Grant No. 2010A140011).

†Corresponding author. E-mail: lynczjg@gmail.com

© 2011 Chinese Physical Society and IOP Publishing Ltd

ions in the TiO_2–SiO_2 mixed material.

In this work, we investigate the structures and photoluminescence (PL) properties of 2 mol% Er^{3+}-doped $5TiO_2$–SiO_2 powders at different annealing temperatures and 2 mol% Er^{3+}-doped TiO_2–SiO_2 with different Ti/Si ratios annealed at 900 °C. The mechanism of visible PL is also discussed.

2. Experiment

2.1. Sample preparation

The samples were prepared by the sol–gel process using tetraethoxysilane (TEOS), ethanol, deionized water, tetra-n-butyl titanate ($Ti(OC_4H_9)_4$), NS $Er(NO_3)_3{\cdot}5H_2O$ as the starting materials. All the raw materials are analytical reagents. A small amount of concentrated hydrochloric acid was added as a catalyst. Since the hydrolysis rate of the $Ti(OC_4H_9)_4$ is greater than that of TEOS, first the TEOS was hydrolyzed with a mixed solution of ethanol and deionized water, followed by stirring for 1 h at about 60 °C. In another container, $Ti(OC_4H_9)_4$ was mixed with the ethanol, deionized water, and hydrochloric acid, then it was added slowly to the TEOS solution and stirred for 3 h at 60 °C. When the solution was cooled down to room temperature, $Er(NO_3)_3{\cdot}5H_2O$ dissolved in ethanol was added to this solution and stirred for 1 h. The solution was aged for 1 day and dried at 70 °C for 60 h. The Er^{3+} amount relative to the total cation concentration (Ti+Si) is 2% for all the samples. Two groups of samples were prepared. The first was annealed at 600, 700, 800, 900, and 1000 °C, separately, for 1 h in air; the second group had different Ti/Si ratios of 10/1, 5/1, 2/1, 1/1, and 1/10 annealed at 900 °C for 1 h in air. The powders were obtained by grinding using an agate mortar.

2.2. Characterization

The X-ray diffraction (XRD) patterns of the samples were obtained by X-ray diffractometry (Rigaku D/Max-IIIC) using Cu Kα radiation. Raman spectra were measured by microspectrascopy (JY-HR800) using a 532-nm Ar^+ ion laser as the exciting light source. The microstructures of the synthesized products were analysed using high resolution transmission electron microscopy (HR-TEM) (JEOL JEM 2010F). PL spectra were measured with a JohnYvon HR800 spectrometer at 325 nm. All measurements for the samples were carried out at room temperature.

3. Results and discussion

Figure 1(a) shows the TEM image of 2 mol% Er^{3+}-doped $5TiO_2$–SiO_2 powders annealed at 900 °C for 1 h. A crystalline area diffracts incident electrons, causing it to be darker in the image than in an amorphous powder. In addition, if two particles are overlapping, the overlapped area will be darker than that of the single particle. The TEM results indicate that the growth and the agglomeration of titania nanoparticles were restrained because of the presence of silica. The soft- and the hard-nanoparticle agglomerates can be produced in the sol–gel process. The soft agglomerates are usually considered as particles held together by weak physical van der Waals forces, while the hard agglomerates are held by stronger chemical sintering bonds.[19] To prevent the agglomerated nanoparticles from forming, we can add a very small number of surfactants. The average size of the spherical TiO_2 particles was about 9 nm in diameter. The crystal structure was identified to be anatase phase using X-ray diffraction. The composite particles consisted of spherical anatase TiO_2 particles surrounded by amorphous SiO_2, which was believed to contain Si–O–Ti. Since the starting solutions were partially hydrolyzed, Si–O–Ti bondings may have formed via the distribution of Ti atoms in O–Si–O chains. A similar observation was made by others.[20] Figure 1(b) shows TiO_2 nanocrystallites homogeneously dispersed in the amorphous SiO_2 matrix. The lattice fringe of ∼0.35 nm was also observed, which corresponds to the lattice spacing of the (101) plane in the anatase phase of TiO_2. The SEAD pattern shows high-grade crystallinity for this sample (Fig. 1(c)).

Typical XRD patterns of 2 mol% Er^{3+}-doped $5TiO_2$–SiO_2 powders appearing at different annealing temperatures (600 °C–1000 °C) are shown in Fig. 2(a). It can clearly be seen that the major phases of all the mixtures were an anatase structure TiO_2 and a weak rutile peak of TiO_2, as well as an amorphous phase of silica-based network identified by a broad peak centred at 22°. No peaks from erbium compound and no shift of the anatase and rutile peaks are detected after doping Er^{3+} ions, indicating that the incorporation of Er^{3+} ions does not change the structures of all the mixed powders. The crystalline sizes are estimated by using Scherrer's equation and the sizes each as the function of annealed temperature are listed in Table 1. This reveals that the crystallite sizes increase from 6.9 nm to 20.7 nm with annealing temperature increasing. The sizes of the samples annealed at 900 °C

are in agreement with the values determined by HR-TEM analysis. This result indicates that the addition of SiO_2 to titania particles decreases the crystallite size and crstallinity by inhibiting the growth of the titania particles. It is well known that the annealing improves the crystallinity of the particles, and the amorphous TiO_2 changes into anatase phase and the anatase phase changes into rutile phase with increasing annealing temperature.[21] The inhibition of SiO_2 from phase transformation causes the nucleation rate to slow down.

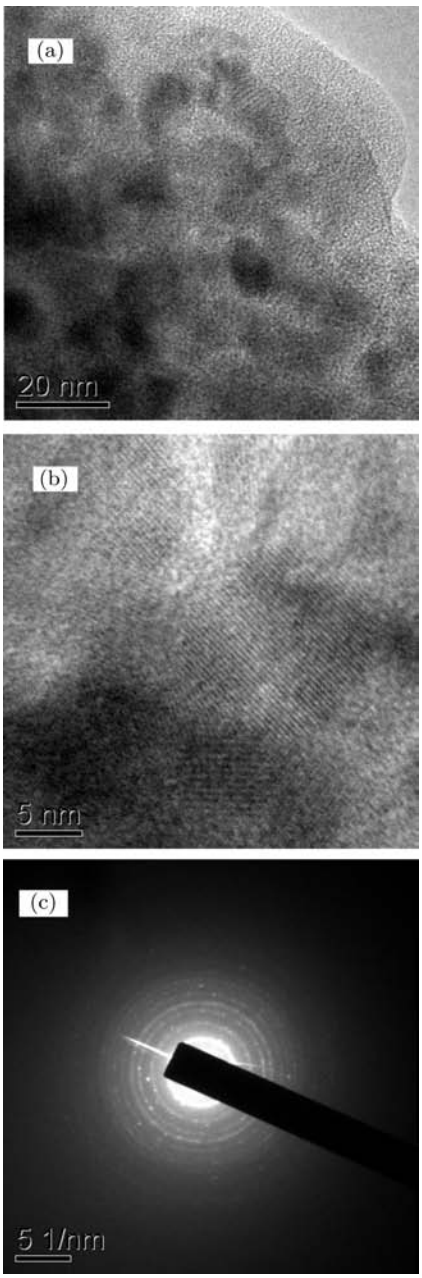


Fig. 1. (a) TEM, (b) HR-TEM, and (c) SEAD images of 2 mol% Er^{3+}-doped $5TiO_2$–SiO_2 powders annealed at 900 °C for 1 h.

Table 1. Grain sizes each as a function of annealed temperature from X-ray diffraction data.

Annealing temperature/°C	Average grain sizes /nm (A(101))
600	6.9
700	7.3
800	8.5
900	9.1
1000	20.7

Figure 2(b) shows XRD patterns of the samples with different Ti/Si ratios, annealed at 900 °C for 1 h. For the sample of 2 mol% Er^{3+}-doped TiO_2–$10SiO_2$ powders, a broad peak around $2\theta = 22°$ corresponds to the (100) plane of the amorphous phase of silica. This is the amorphous form of the silica phase (JCPDS 39-1425), which exists as a crystallized form above 1600 °C. Thus the sample is a typical amorphous phase.[22] It is known that TiO_2 is formed as a stable tetragonal anatase under heat treatment at 700 °C, and a tetragonal rutile structure above 700 °C.[23]

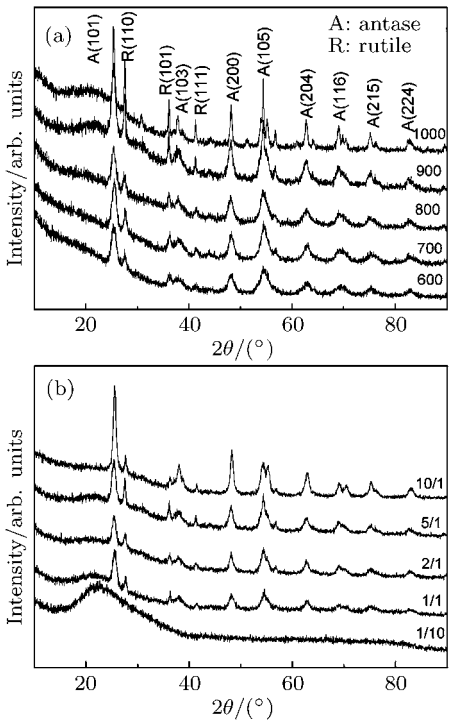


Fig. 2. (a) The XRD patterns of 2 mol% Er^{3+}-doped $5TiO_2$–SiO_2 prepared at different annealing temperatures (600 °C–1000 °C) for 1 h. (b) The XRD patterns of 2 mol% Er^{3+}-doped different ratios of Ti/Si annealed at 900 °C for 1 h.

In the present paper, despite the relatively high heat treatment temperature of 900 °C, the mixed form of the rutile and anatase structures is observed at a

higher Ti ratio. We can surmise that the TiO_2 rutile structure is prevented from forming due to the presence of SiO_2, and thus the phase transition temperature is shifted to a higher temperature region. This result suggests that the formation of anatase phase would be extended to higher temperatures in TiO_2/SiO_2 composite powders. The sizes each as a function of Ti/Si ratios are listed in Table 2. The average particle size of TiO_2 increases from 7.1 nm to 13.2 nm with increasing Ti/Si ratio as determined by Scherrer's equation.

Table 2. Grain sizes each as a function of the Ti/Si ratio from X-ray diffraction data.

Ti/Si ratio /at.%	Average grain sizes/nm (A(101))
1/1	7.1
2/1	7.7
5/1	9.1
10/1	13.2

Figure 3(a) shows the Raman spectra of 2 mol% Er^{3+}-doped $5TiO_2$–SiO_2 prepared at different annealing temperatures (600 °C–1000 °C). It can be see that the formation of an anatase phase is evident from the characteristic anatase Raman modes at 136 cm^{-1}(E_g), 392 cm^{-1} (B_{1g}), 512 cm^{-1} (B_{2g}), and 630 cm^{-1} (E_g). Of these, the intensity of the band at 136 cm^{-1} is extremely strong and the presence of this band is an indication of the formation of anantase.[24] The band at 610 cm^{-1} (E_g), characteristic of the rutile phase, is also observed on all the spectra.

The Raman spectroscopy of amorphous silica usually presents a large band at 440 cm^{-1} and weaker bands located at 492 cm^{-1} and 605 cm^{-1}. The band at 440 cm^{-1} has been assigned to the combination of the Si–O–Si and O–Si–O bond bending vibrations. The bands at 488 cm^{-1} and 605 cm^{-1} have been attributed to defects in the network.[25–27] So the broad band at 550 cm^{-1} is due to superposition of the crystallization TiO_2 and amorphous SiO_2. From these various data, it can be concluded that the nanocomposite nature of the prepared samples consists of amorphous silica and crystallization TiO_2.

Figure 3(b) shows the Raman spectra of 2 mol% Er^{3+}-doped samples with different ratios of Ti/Si, annealed at 900 °C. There is no Raman peak for the 2 mol % Er^{3+}-doped TiO_2-$10SiO_2$ powders. This result is in agreement with the XRD (see Fig. 2(b)). The intensity of the Raman peak at 136 cm^{-1} associated with the anatase phase increases with increasing Ti/Si ratio. The result shows that the introduction of SiO_2 inhibits the crystallization of TiO_2 and elevates the phase transition temperature. The Raman peak of the E_g mode of TiO_2 shifts toward a lower wavenumber with increasing Ti/Si ratio.[28] The strain is caused by the surface coating, which may be responsible for the Raman shift.

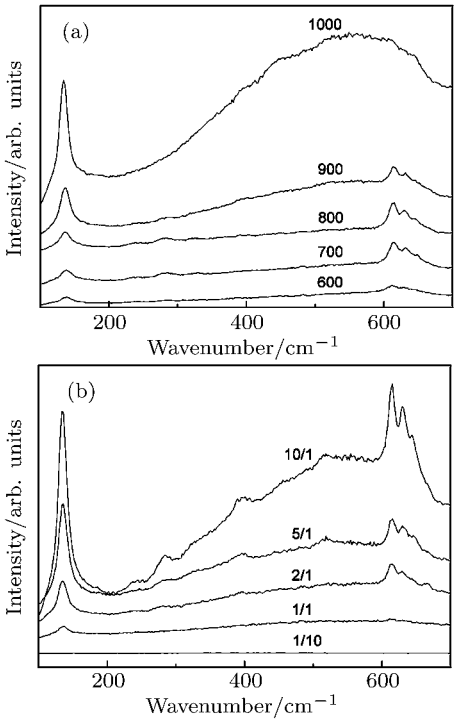


Fig. 3. (a) Raman spectra of 2 mol% Er^{3+}-doped $5TiO_2$–SiO_2 prepared at different annealing temperatures (600 °C–1000 °C) for 1 h. (b) Raman spectra of 2 mol% Er^{3+}-doped different ratios of Ti/Si, annealed at 900 °C for 1 h.

Figure 4(a) shows the PL spectra of 2 mol% Er^{3+}-doped $5TiO_2$–SiO_2 prepared at different annealing temperatures (600 °C–1000 °C) for 1 h under the excitation of 325 nm He–Cd laser, the pumping laser power is 5 mW. There are two main emission bands in Fig. 4(a), which correspond to green emission (523 nm, 545 nm) and red emission (660 nm) regions, due to the intra-4f transitions of $^2H_{11/2}/^4S_{3/2} \rightarrow ^4I_{15/2}$ and $^4F_{9/2} \rightarrow ^4I_{15/2}$, respectively. The energy level diagram of Er^{3+} ions in the visible region is given in Fig. 5. The UV energy absorbed by samples will transfer through the defect states of TiO_2 to Er^{3+} ions, resulting in visible emission. The fluorescence at 800 nm was not found, because excited Er^{3+} ions in the $^4I_{9/2}$ level decayed to the $^4I_{11/2}$ state rapidly through the non-radiative transition by emission of phonons.[29] When the annealing temperature increases from 600 °C to 800 °C, the intensity of the visible emission increases

in Fig. 4(a). This is due to the fact that the residual organics are decomposed and the defects decrease. The intensity of the emission is the strongest at the annealing temperature of 800 °C because the TiO_2 nanoparticles are better crystallized, and the influence of quenching is reduced. When the annealing temperature is higher than 800 °C, the intensity of the luminescence is decreasing accompanying an emission with a broad emission band at around 530 nm. We can explain it as follows. With the rutile phase increasing, the defect states increase. This can be ascribed to the defect states, which reduces the luminescence of Er^{3+} ions due to lower efficiency of energy transfers from the defect states to Er^{3+} ions.

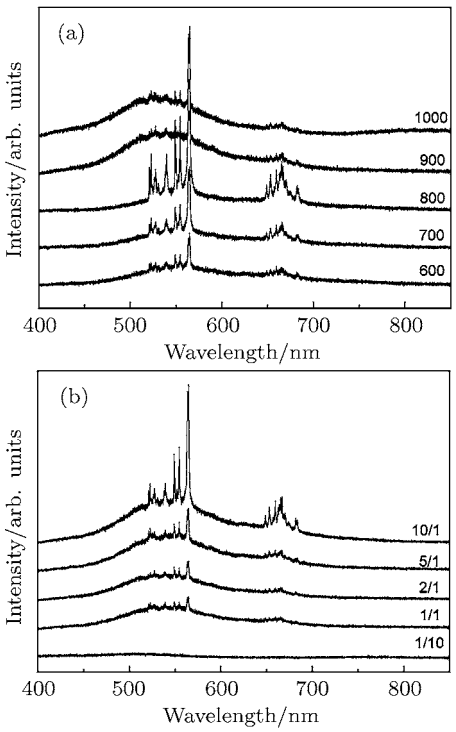


Fig. 4. (a) PL spectra of 2 mol% Er^{3+}-doped $5TiO_2$–SiO_2 prepared at different annealing temperatures (600 °C–1000 °C) for 1 h. (b) PL spectra of 2 mol% Er^{3+}-doped different ratios of Ti/Si, annealed at 900 °C for 1 h.

Figure 4(b) shows the PL spectra of the samples with different ratios of Ti/Si, annealed at 900 °C for 1 h. The spectra show that the intensity of the Er^{3+} ion visible emission increases with increasing Ti/Si ratio. The weakest luminescence intensity corresponds to the lowest TiO_2 content, and as TiO_2 increases, the Er^{3+} concentration quenching effect of PL vanishes, leading to enhanced luminescence intensity. This behaviour can be explained in terms of the affinity of Er^{3+} ions introduced into the TiO_2 lattice. Thus with an increase in TiO_2 content, the ions of Er^{3+} become more separated and the interactions among the Er^{3+} ions are less feasible. On the other hand, the enhancement of PL intensity can be ascribed to the effective energy transfer from TiO_2 nanoparticles to the rare-earth ions due to the strong interaction between photo-generated electrons in TiO_2 nanoparticles and nearby Er^{3+} ions. With Ti/Si ratio increasing, the number of TiO_2 nanoparticles increases, which is more favourable for energy transfer from the excited TiO_2 nanoparticles to the nearby Er^{3+} ions. Meanwhile, more TiO_2 nanoparticles mean that the exciting light is absorbed more effectively and more electrons transfer nonradiatively to the luminescent centres (Er^{3+} ions).

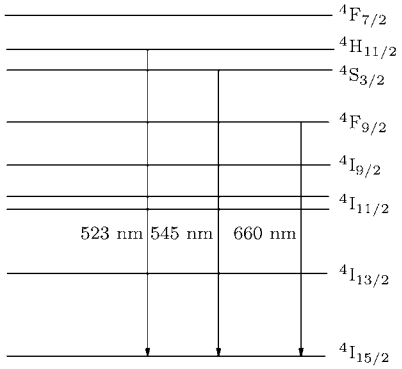


Fig. 5. Energy level diagram of Er^{3+} ions in the visible region.

4. Conclusion

In this paper, Er^{3+}-doped TiO_2–SiO_2 powders with nano-crystalline TiO_2 are obtained by the sol–gel method. The Ti/Si ratios change from 1/10 to 10/1 with the samples annealed at 900 °C for 1 h, and the 2 mol% Er^{3+}-doped $5TiO_2$–SiO_2 powders are annealed at different temperatures (600 °C–1000 °C). The effects of annealing and Ti/Si ratio on the structure and PL properties of the powders are studied. Visible PLs peaked at 523 nm, 545 nm, and 660 nm are detected, which are ascribed to $^2H_{11/2} \rightarrow {}^4I_{15/2}$, $^4S_{3/2} \rightarrow {}^4I_{15/2}$, and $^4F_{9/2} \rightarrow {}^4I_{15/2}$ transitions of Er^{3+} ions, respectively. The obtained results reveal that with the annealing temperature increasing, the intensities of the visible emissions are first increasing then decreasing. These are ascribed to the various defect states. With Ti/Si ratio increasing, the number of TiO_2 nanoparticles increases, which is more favourable for energy transfer from the excited TiO_2 nanoparticles to the nearby Er^{3+} ions.

References

[1] Kyatskaya S, Mascaros J R, Bogani L, Hennrich F, Kappes M, Wernsdorfer W and Ruben M 2009 *J. Am. Chem. Soc.* **131** 15143

[2] Cui C E, Wang S and Huang P 2009 *Acta. Phys. Sin.* **58** 3565 (in Chinese)

[3] Smet P F and Poelman D P 2009 *J. Phys.* D: *Appl. Phys.* **42** 095306

[4] Wu J C, Tian Q W, Hu H, Xia Q, Zou Y, Li F Y, Yi T and Huang C H 2009 *Chem. Commun.* **27** 4100

[5] Dahal R, Ugolini C, Lin J Y, Jiang H X and Zavada J M 2009 *Appl. Phys. Lett.* **95** 111109

[6] Kumar A, Babu S, Karakoti A S, Schulte A and Seal S 2009 *Langmuir.* **25** 10998

[7] Kanjilal A, Rebohle L, Voelskow M, Skorupa W and Helm M 2009 *Appl. Phys. Lett.* **94** 051903

[8] Ding W C, Liu Y, Zhang Y, Guo J Q, Zuo Y H, Cheng B W, Yu J Z and Wang Q M 2009 *Chin. Phys.* B **18** 3044

[9] You H P and Nogami M 2004 *J. Phys. Chem.* B **108** 12003

[10] Contreras J C, Nava M A, Garcia O B, Rojas R A and Felix M V 2006 *Opt. Mater.* **29** 38

[11] Xu N P, Shi Z F, Fan Y Q, Dong J H, Shi J and Hu M Z 1999 *Ind. Eng. Chem. Res.* **38** 373

[12] Fujihara K, Kumar A, Jose R, Ramakrishna S and Uchida S 2007 *Nanotechnology* **18** 365709

[13] Zhang Y Z, Wu L H, Xie E Q, Duan H G, Han W H and Zhao J G 2009 *J. Power Sources* **189** 1256

[14] Macak J M, Zlamal M, Krysa J and Schmuki P 2007 *Small* **3** 300

[15] Biswas P K, Devi P S, Chakraborty P K, Chatterjee A, Ganguli D, Kamath M P and Joshi A S 2003 *J. Mater. Sci. Lett.* **22** 181

[16] Grodz I Z, Mista W, Strek W, Bukowska E, Hermanowicz K and Maruszewski K 2004 *Opt. Mater.* **26** 207

[17] Zhang X T, Fujishima A, Jin M, Emeline A V and Murakami T 2006 *J. Phys. Chem.* B **110** 25142

[18] Zaharescu M, Barau A, Predoana L, Gartner M, Anastasescu M, Mrazek J, Kasik I and Matejec V 2008 *J. Non-Cryst. Solids* **354** 693

[19] Kammler H K, Beaucage G, Kohls D J, Agashe N and Ilavsky J 2005 *J. Appl. Phys.* **97** 054309

[20] Kwon C H, Kim J H, Jung I S, Shin H and Yoon K H 2003 *Ceramics International* **29** 851

[21] Lee M S, Lee G D, Park S S and Hong S S 2003 *J. Ind. Eng. Chem.* **9** 89

[22] You H P and Nogami M 2006 *J. Alloy Compd.* **408** 796

[23] Segawa H, Fukuyoshi J, Tanaka K and Yoshida K 2003 *J. Mater. Sci. Lett.* **22** 687

[24] Gao X, Bare S R, Fierro J L G, Banares M A and Wachs I E 1998 *J. Phys. Chem.* B **102** 5653

[25] Kailer A, Nickel K G and Gogotsi Y G 1999 *J. Raman Spectrosc.* **30** 939

[26] Best M F and Condrate Sr R A 1985 *J. Mater. Sci. Lett.* **4** 994

[27] Bosc F, Ayral A and Guizard C 2006 *Thin Solid Films* **495** 252

[28] Gotic M, Ivanda M, Popovic S, Music S, Sekulic A, Turkovic A and Furic K 1997 *J. Raman Spectrosc.* **28** 555

[29] Maeda N, Wada N, Onoda H, Maegawa A and Kojima K 2003 *Thin Solid Films* **445** 382